ACS OMEGA

Open Access

This article is licensed under CC-BY-NC-ND 4.0

http://pubs.acs.org/journal/acsodf

Article

Investigating the Mechanism of the Fuzheng Huayu Formula in Treating Cirrhosis through Network Pharmacology, Molecular Docking, and Experimental Verification

Ruixue Yu, Run Shi, Jinghua Chen, Xinhua Zheng, and Ruitao Yu*

Cite This: *ACS Omega* 2025, 10, 19019−19032

Read Online

ACCESS | Metrics & More | Article Recommendations | Supporting Information

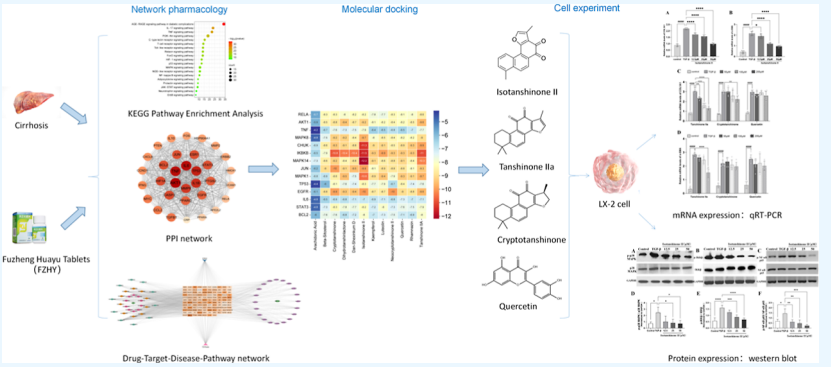

ABSTRACT: Cirrhosis, characterized by liver fibrosis and structural remodeling, is a leading cause of liver cancer. The Fuzheng Huayu formula (FZHY) has been approved for treating liver fibrosis in China since 2002, but its effects and mechanisms on cirrhosis remain largely unknown. This study employed network pharmacology, molecular docking, and in vitro experiments to elucidate the specific mechanisms of FZHY against liver cirrhosis. First, intersecting genes between FZHY and cirrhosis were obtained from the Chinese Medicine System Pharmacology Database, the Swiss Target Prediction online platform, UniProt, GeneCards, DisGeNET, and OMIM. The STRING database was used to construct a protein−protein interaction network. Subsequently, Gene Ontology functional annotation and Kyoto Encyclopedia of Genes and Genomes (KEGG) pathway analysis were performed, followed by molecular docking analysis to verify binding affinities between active ingredients and candidate targets. These analyses provided a theoretical basis for subsequent experimental research. Finally, we identified 117 FZHY target genes associated with cirrhosis and constructed a drug−component−target−cirrhosis-pathway network. Enrichment analysis revealed the AGE-RAGE signaling pathway in diabetic complications as a key pathway. Molecular docking showed that Isotanshinone II had the highest affinity for CHUK, IKBKB, and MAPK14. In vitro experiments demonstrated that Isotanshinone II dose-dependently reduced the mRNA expression of COL1A1 and α-SMA, as well as the protein levels of MAPK p38, IKKβ, and NF-κB p65 in LX-2 cells. These results revealed the underlying mechanism by which Isotanshinone II in FZHY inhibited LX-2 cell activation and collagen production through suppression of the MAPK/NF-κB signaling pathway. These findings support Isotanshinone II as a promising compound for cirrhosis targeting the MAPK/NF-κB pathway. Further research is warranted to explore the bioavailability of Isotanshinone II and to optimize its structure for clinical applications.

1. INTRODUCTION

Cirrhosis, a chronic liver disease characterized by diffuse fibrosis and structural remodeling, is a leading cause of liver-related mortality worldwide. It primarily arises from chronic liver injuries induced by hepatitis B and C virus (HBV/HCV) infections, chronic alcohol abuse, or metabolic dysfunction-associated steatotic liver disease (MASLD). Patients with cirrhosis typically present with complications such as portal hypertension, ascites, hepatic encephalopathy, and multiorgan dysfunction, all of which severely impact prognosis.[1] During the progression of cirrhosis, the activation of hepatic stellate cells (HSCs) drives excessive extracellular matrix (ECM) deposition, while continuous hepatocyte damage and repair further exacerbate liver fibrosis, ultimately leading to cirrhosis.[2] Statistical data indicate that 2.5% of the global deaths in 2021 were cirrhosis-related.[3] Currently, therapeutic options for cirrhosis are limited, primarily involving etiological treatment,

Received: February 8, 2025
Revised: April 16, 2025
Accepted: April 17, 2025
Published: April 29, 2025

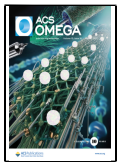

ACS Publications

© 2025 The Authors. Published by American Chemical Society

antifibrotic therapy, complication management, and liver transplantation.[4] However, treatment efficacy and prognosis remain suboptimal, highlighting the critical importance of early prevention and diagnosis.

Traditional Chinese Medicine (TCM), with its holistic approach and rich history of treating chronic diseases, offers a promising alternative. Fuzheng Huayu tablets (FZHY), the tablet form of a well-established TCM formula approved by the Chinese State Food and Drug Administration (No. Z20050546) in 2002, have been extensively used in China for the treatment of liver fibrosis and cirrhosis.[5] Composed of six herbal components including *Salvia miltiorrhiza Bge* (*Danshen*), *Persicae Semen* (*Taoren*), *Ophiocordyceps sinensis* (*Dongchong-xiacao*), *Gynostemma Pentaphyllum* (*Jiaogulan*), *Schisandrae Chinensis* (*Wuweizi*), and *Pini Pollen* (*Songhuafen*), FZHY has demonstrated dual therapeutic effects: delaying fibrosis progression and alleviating clinical symptoms.[6] Clinical studies have shown that FZHY can reduce Child-Turcotte-Pugh (CTP) scores and exhibit favorable antifibrotic effects.[7] Furthermore, basic research and clinical trials have confirmed its antifibrotic activity.[8,9] Notably, a U.S.-based multicenter Phase II trial confirmed its efficacy in hepatitis C patients,[10] while mechanistic studies linked its activity to macrophage polarization modulation.[11,12] However, systems-level mechanisms involving multicomponent synergy and pathway crosstalk remain elusive, hindering global clinical translation.

TCM formulas, characterized by their multicomponent nature, exhibit intricate mechanisms of action that involve multitarget and multipathway regulation. Network pharmacology, integrating multiomics data, bioinformatics tools, and systems biology principles, provides a powerful framework for unraveling the complex interactions between drugs and their biological targets. By constructing comprehensive molecular networks that link drugs, targets, and associated diseases, network pharmacology enables the identification of both potential therapeutic mechanisms and novel drug candidates. Furthermore, molecular docking simulated interactions between molecules, predicting binding affinity and binding modes. Through network pharmacology and molecular docking, the bioactive components of FZHY and their targets were identified, revealing the protein structures influenced by the active components and validating the proposed mechanisms.

In this study, we elucidated the potential mechanism of FZHY against cirrhosis by integrating a network pharmacology predictions, molecular docking, and in vitro experiments. Specifically, we constructed a comprehensive network that captured the interactions among the active compounds of FZHY, their potential targets, and the key pathways involved in cirrhosis. Furthermore, we conducted molecular docking simulations and in vitro cell experiments to evaluate the binding affinity and pharmacological mechanisms of the identified active compounds. By integrating these results, we proposed a comprehensive mechanism for the therapeutic effects of FZHY in the treatment of cirrhosis.

2. MATERIALS AND METHODS

2.1. Screening of the Active Components and Targets of FZHY. Active components and targets of *Danshen* (DS), *Taoren* (TR), *Dongchong-xiacao* (DCXC), *Jiaogulan* (JGL), *Wuweizi* (WWZ), and *Songhuafen* (SHF) were identified through the TCMSP database (http://old.tcmsp-e.com/tcmsp.php). Because the main dosage forms of FZHY were capsules or tablets, the initial screening of active ingredients was based on the criteria of drug-likeness (DL) $\geq$ 0.18 and oral bioavailability (OB) $\geq$ 30%. To supplement compounds that met the established criteria for DL and OB, especially those with suitable gastrointestinal absorption (GI absorption), data from the Chinese National Knowledge Infrastructure (CNKI) database (https://www.cnki.net) and the SwissTargetPrediction online platform (http://www.swisstargetprediction.ch/) were integrated. By integrating the UniProt database (https://www.uniprot.org/), predicted protein targets were converted to target names and standardized to official gene symbols, with duplicate and invalid targets removed. Subsequently, the eligible components were summarized as a comprehensive list of the active components and targets for FZHY.

2.2. Acquisition of Cirrhosis Target Genes. The keyword "cirrhosis" was entered into the following databases: TCMSP, GeneCards (https://www.genecards.org/), DisGeNET (https://www.disgenet.org/home/), and Online Mendelian Inheritance in Man (OMIM, https://omim.org/) to identify cirrhosis-related target genes. Target genes were selected from the GeneCards database based on a relevance score $\geq$10 and from the DisGeNET database based on a gene−disease association threshold (score_gda) $\geq$ 0.3. After merging targets from these databases, duplicates were removed to finalize the list of cirrhosis targets.

2.3. Construction of the "Component-Target" Network. The Venny 2.1 tool (https://bioinfogp.cnb.csic.es/tools/venny/) was used to generate a Venn diagram and obtain the intersecting targets between the targets of each active component in FZHY and those of cirrhosis. These intersecting targets represented the potential therapeutic targets of FZHY against cirrhosis, which was used for subsequent analysis. Cytoscape 3.10.2 software was employed to construct the "Component-Target" network diagram. In this diagram, nodes represent the drugs, components, targets, and diseases, while edges indicate the interactions and relationships among them.

2.4. Analysis of the Protein−Protein Interaction (PPI) Network. Intersection target genes were imported into the STRING 12.0 platform, with the "multiple proteins" mode selected for "*Homo sapiens*" and the "full STRING network" chosen as the network type. The required confidence score was set to $\geq$0.4 for the construction of the protein-protein interaction (PPI) network. The Cytoscape 3.10.2 software was applied to conduct topological analysis and identify the core targets of the PPI networks. The top genes were identified as the core targets of FZHY for the treatment of cirrhosis and were used for the enrichment report.

2.5. Analysis of Pathway and Function Enrichment. Core targets of FZHY in cirrhosis were uploaded to the DAVID database (https://david.ncifcrf.gov/tools.jsp). Gene Ontology (GO) functional enrichment analysis and Kyoto Encyclopedia of Genes and Genomes (KEGG) pathway enrichment analysis were performed with a significance threshold of $p \leq 0.05$. The analyses encompassed four domains: biological processes (BP), molecular function (MF), cellular component (CC), and metabolic pathways. The KEGG analysis results were sorted in ascending order according to the p-value, and only results with $p < 0.05$ were retained. The "Pathway Secondary Classification Summary" tool on the Bioinformatics Platform (http://bioinformatics.com.cn/) was then used for pathway classification analysis. Finally, based on the purpose of this study, the most representative classification was selected, and graphs were generated based on the results of Count and GeneRatio. The

https://doi.org/10.1021/acsomega.5c01225
ACS Omega 2025, 10, 19019−19032

Table 1. Sequence of COL1A1, α-SMA, and GAPDH Primers for qRT-PCR

gene	forward (5′ → 3′)	reverse (5′ → 3′)	product size (bp)
COL1A1	AAGCTGGAAAACCTGGTCGT	AGCACCATCATTTCCACGAG	154
α-SMA	CCTATCCCCGGGACTAAGAC	CCATCACCCCCTGATGTCTG	196
GAPDH	CAGGAGGCATTGCTGATGAT	CAGGAGGCATTGCTGATGAT	208

Bioinformatics Platform was used for visualization of these enrichment results.

2.6. Construction of the "Drug-Target-Disease-Pathway" Regulatory Network. The common target information, GO, and KEGG enrichment analysis results were imported into Cytoscape 3.10.2 software to construct the "drug-target-disease-pathway" regulatory network. The results of network analysis were obtained by the Analyze Network tool, and genes were sorted by descending degree values. Based on the obtained PPI network information and the secondary classification summary of pathways, the top 14 target genes were selected for further molecular docking studies as the core targets.

2.7. Docking Simulation Analysis of Active Components and Key Targets. The 3D structures of the main active components were downloaded from the PubChem database (https://pubchem.ncbi.nlm.nih.gov), and energy minimization was performed using the MM2 calculation function in Chem3D 20.0 software to obtain the initial conformation. Twelve core targets with high degree values were selected from the STRING database as receptors. The PDB files of receptors with high resolution (≤2.5 Å) and physiological pH (7.0−7.4) for *H. sapiens* were downloaded from the RCSB Protein Data Bank (https://www.rcsb.org). Water molecules and co-crystallized ligands were removed using PyMOL 2.4.1 software. Subsequently, AutoDockTools 1.5.7 was employed to define the position and dimensions of the grid box based on the receptor binding site. Molecular docking analysis was then performed for all receptor-ligand combinations. The docking results were visualized using Discovery Studio 2021.

2.8. Cell Culture and Drug Source. Human HSCs (LX-2, Procell Life Science & Technology, Wuhan, China) were cultured in Dulbecco's modified Eagle's medium (DMEM, Thermo Fisher Scientific, Waltham, USA) supplemented with 10% fetal bovine serum (Thermo Fisher Scientific, Waltham, MA, USA), 100 U/mL penicillin, and 50 U/mL streptomycin (TBD Science, Tianjin, China) at 37 °C in 5% CO_2. After 48 h of treatment under these conditions, the cells were harvested for cell viability assays or Western blot analysis. Isotanshinone II (CAS No.: 98249-39-9), Tanshinone IIA (CAS No.: 568-72-9), Cryptotanshinone (CAS No.: 35825-57-1), and Quercetin (CAS No.: 117-39-5) were purchased from MedChemExpress (MCE, Monmouth Junction, NJ, USA). All compounds were dissolved in dimethyl sulfoxide (DMSO, final concentration <0.1%) and diluted with DMEM prior to use.

2.9. Cell Viability Assay. Cell viability was analyzed using the Cell Counting Kit-8 (CCK-8, Nanjing Jiancheng Bioengineering Institute, Nanjing, China) according to the manufacturer's protocol. LX-2 cells were seeded at a density of 5,000 cells per well in a 96-well plate. After adhesion, the cells were incubated with different concentrations of Isotanshinone II, Tanshinone IIA, Cryptotanshinone, and Quercetin (HPLC-grade reference substances, purity ≥98%, purchased from Nanjing Dirge Pharmaceutical Technology, Nanjing, China) for 24 h. The tested concentrations were 25, 50, 100, 200, 400, and 800 μmol/L. Subsequently, the cells were washed twice with phosphate-buffered saline (PBS) and incubated with 1:10 diluted CCK-8 reagent in serum-free medium for 2 h at 37 °C. Absorbance was measured at 450 nm using a Multiskan microplate reader (Thermo Fisher Scientific, Waltham, USA). The experiment was repeated three times independently, with each condition tested in triplicate wells.

2.10. qRT-PCR Analysis of COL1A1 Expression in LX-2 Cells. The control group of LX-2 cells was treated with 0.1% DMSO, while the model group and treatment group cells were co-incubated with human transforming growth factor-β 1 (TGF-β1), Isotanshinone II, Tanshinone IIA, Cryptotanshinone, and Quercetin for 48 h, respectively. Cells from each group were collected, and total RNA was extracted using an RNA extraction kit (Takara Bio, Tokyo, Japan). RNA concentration was measured spectrophotometrically, and the extracted RNA was reverse-transcribed into cDNA using a PrimeScript RT reagent kit (Takara Bio, Tokyo, Japan). The cDNA was amplified with a SYBR Green-based amplification kit (Takara Bio, Tokyo, Japan) and primers using a polymerase chain reaction (PCR). The reaction conditions were 95 °C for 1 min, followed by 95 °C for 20 s, 60 °C for 45 s, for a total of 40 cycles, and a final extension at 95 °C for 1 min. Data were analyzed using the $2^{-\Delta\Delta CT}$ method. The primer sequences are listed in Table 1.

2.11. Western Blotting Analysis. Protein expression of p38 MAPK, IKKβ, and NF-κB p65 in each group was measured by western blotting. LX-2 cells were washed with cold PBS, lysed in RIPA buffer (Beyotime Biotechnology, Shanghai, China), incubated on ice for 20 min, and centrifuged for 5 min at 500 rpm. Protein concentration was quantified using a BCA protein assay kit (Beyotime Biotechnology, Shanghai, China). Proteins were separated by SDS-PAGE (Beyotime Biotechnology, Shanghai, China) and transferred to PVDF membranes by the MiniBlot Electrophoretic Transfer System (Beyotime Biotechnology, Shanghai, China). Membranes were blocked with 5% skim milk for 2 h and incubated overnight at 4 °C with the following primary antibodies: polyclonal rabbit antihuman TGF-β1 (1:1000, Boster Biological Technology, Wuhan, China), GAPDH (1:20,000, Boster Biological Technology, Wuhan, China), p38 MAPK (1:1000, Boster Biological Technology, Wuhan, China), p-p38 MAPK (1:1000, Boster Biological Technology, Wuhan, China), IKKβ (1:1000, Boster Biological Technology, Wuhan, China), *p*-IKKβ (1:2000, ABclonal, Wuhan, China), NF-κB (1:1000, Boster Biological Technology, Wuhan, China), and phospho−NF−κB p65- (1:2000, Cell Signaling Technology, Danvers, MA, USA). After washing with Tris-buffered saline with Tween 20 (TBST) three times (10 min each), membranes were incubated with HRP-conjugated goat anti-rabbit secondary antibody (1:3000, Boster Biological Technology, Wuhan, China) at room temperature for 1 h. The membranes were washed again with TBST for 10 min × 3 times and incubated with ECL chemiluminescence substrates (Boster Biological Technology, Wuhan, China). Finally, the bands were quantified by a ChemiDoc XRS+ imaging system (Bio-Rad Laboratories, Hercules, USA).

2.12. Statistical Analysis. Experimental data were statistically analyzed by using GraphPad Prism 10.3.1 software and

https://doi.org/10.1021/acsomega.5c01225
ACS Omega 2025, 10, 19019−19032

SPSS 20.0 software. One-way ANOVA was applied to assess differences in the experimental data between groups. Experimental data are presented as mean ± standard deviation (SD), and statistical significance was set at $p < 0.05$.

3. RESULTS

3.1. Selection of Active Ingredients, Targets of FZHY, and Targets of Cirrhosis. Based on the criteria of OB ≥ 30% and DL ≥ 0.18, the number of active components identified from each herb in FZHY was as follows: *Wuweizi* (WWZ): 21,

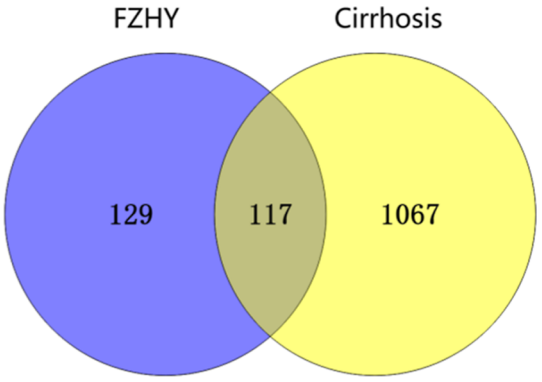

Figure 1. Venn diagram of overlapping targets between Fuzheng Huayu and cirrhosis.

Table 2. Top 12 Active Ingredients in Terms of Degree

serial number	compound name	degree	Chinese medicinal herb belongs to
MOL000098	quercetin	88	*Gynostemmae Pentaphyllum* (JGL)
MOL000006	luteolin	40	*Salvia miltiorrhiza Bge* (DS)
MOL000422	kaempferol	35	*Pini pollen* (SHF)
MOL007154	tanshinone IIA	22	*Salvia miltiorrhiza Bge* (DS)
MOL001439	arachidonic acid	18	*Ophiocordyceps sinensis* (DCXC)
MOL000358	*β*-sitosterol	12	*Ophiocordyceps sinensis* (DCXC), *Persicae semen* (TR)
MOL007093	danshexinkum D	11	*Salvia miltiorrhiza Bge* (DS)
MOL007100	dihydrotanshinlactone	11	*Salvia miltiorrhiza Bge* (DS)
MOL000351	rhamnazin	11	*Gynostemmae Pentaphyllum* (JGL)
MOL007088	cryptotanshinone	10	*Salvia miltiorrhiza Bge* (DS)
MOL007111	isotanshinone II	10	*Salvia miltiorrhiza Bge* (DS)
MOL007124	neocryptotanshinone II	10	*Salvia miltiorrhiza Bge* (DS)

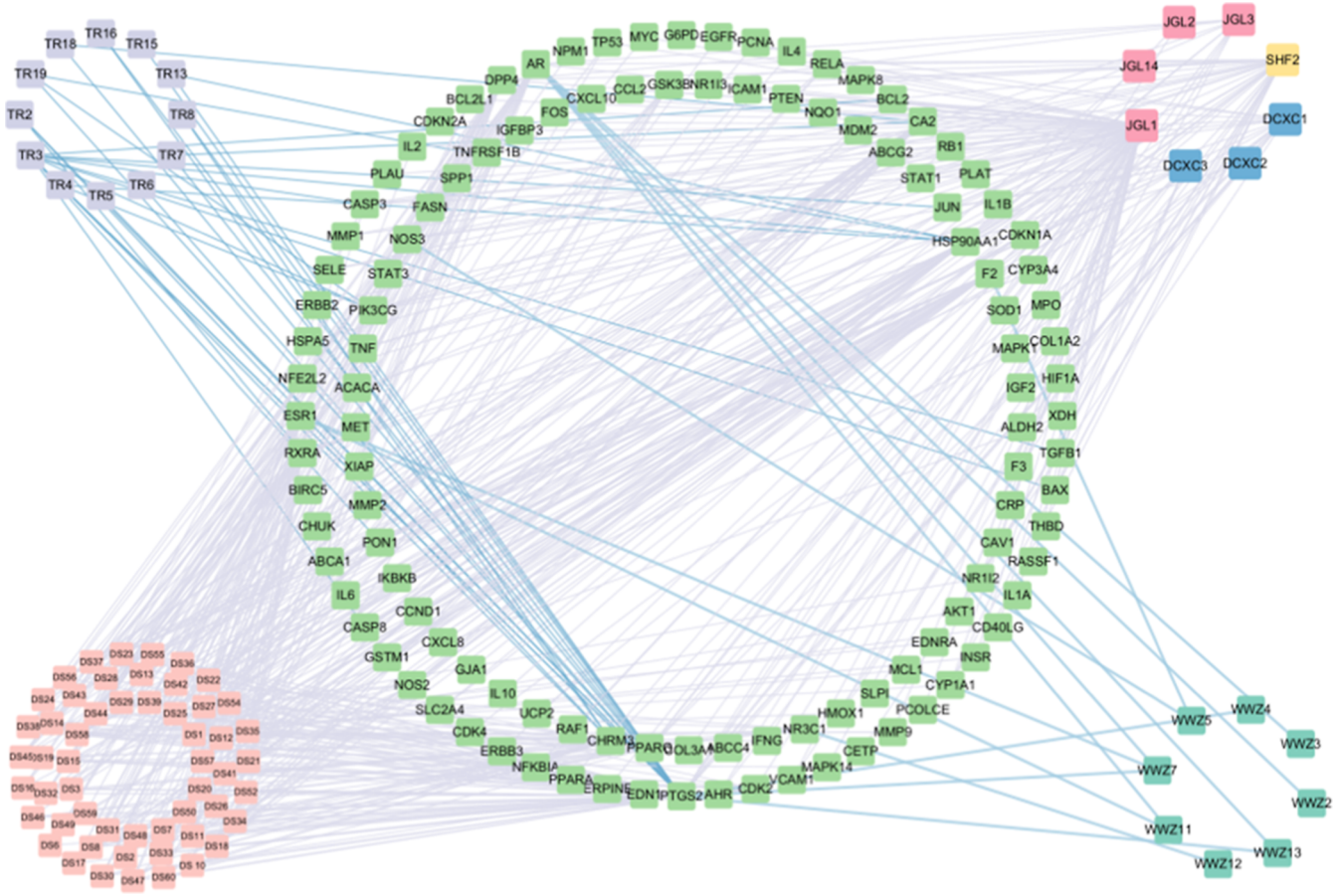

Figure 2. Active ingredient−target network of Fuzheng Huayu in cirrhosis treatment. The network comprises 83 components and 117 shared targets between Fuzheng Huayu and cirrhosis. Edges indicate component−target interactions. Targets located within the central green circles represent overlapping genes between Fuzheng Huayu and cirrhosis, while peripheral nodes denote active components.

https://doi.org/10.1021/acsomega.5c01225
ACS Omega 2025, 10, 19019−19032

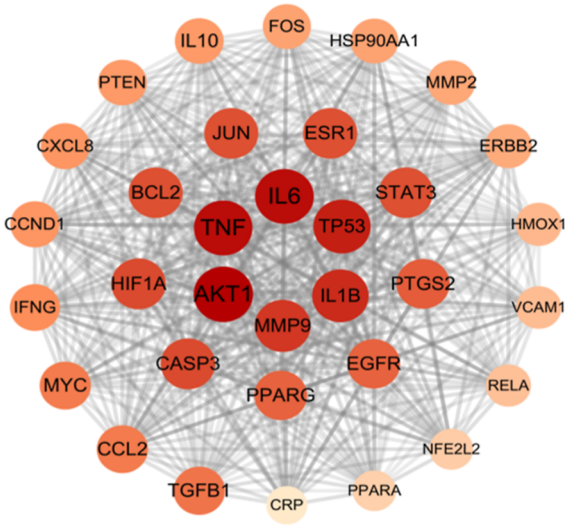

Figure 3. Protein−protein interaction (PPI) network of Fuzheng Huayu's key targets against treating cirrhosis. Red nodes within the two inner circles denote the top 15 targets ranked by degree centrality. Node size reflects interaction frequency, and color intensity indicates statistical significance.

Danshen (DS): 65, *Dongchongxiacao* (DCXC): 7, *Jiaogulan* (JGL): 24, *Songhuafen* (SHF): 2, and *Taoren* (TR): 23 (Table S1). After removing duplicate components, a total of 139 unique active components of the FZHY remained. Potential targets of these components were retrieved from the TCMSP, UniProt Database, PubChem, and SwissTargetPrediction databases, yielding 246 targets. Cirrhosis-related targets (n = 1184) were collected from GeneCards, OMIM, DisGeNET, and DrugBank databases. The intersection between FZHY component targets and cirrhosis-related targets revealed 117 shared targets, and a Venn diagram was constructed to illustrate this (Figure 1).

3.2. Active Ingredient−Target Network Analysis for Identifying Key Components. A "component-target" network was constructed using Cytoscape 3.10.2 software by integrating the active components with the intersecting targets (Figure 2). In the Fuzheng Huayu formula, 83 components were identified to share common targets with cirrhosis-associated genes. The Analyze Network tool was utilized to evaluate node importance based on degree centrality, with higher values indicating greater network significance. The analysis revealed that the active components with the highest degree values include quercetin, luteolin, kaempferol, tanshinone IIA, arachidonic acid, β-sitosterol, danshexinkum D, dihydrotanshinlactone, rhamnazin, cryptotanshinone, isotanshinone II, and neocryptotanshinone II (Table S2). These 12 active components were hypothesized to represent the key therapeutic elements of Fuzheng Huayu in treating cirrhosis (Table 2).

3.3. PPI Network Construction and Key Target Analysis. The targets of FZHY against cirrhosis were imported into the STRING database, and a protein-protein interaction (PPI) network was constructed using Cytoscape 3.10.2 software. The CentiScape 2.2 plugin was used to calculate the median values of betweenness centrality (BC), closeness centrality (CC), and degree centrality (DC) for each node, which served as screening thresholds.[13] Thirty-three target proteins were identified with all three centrality values exceeding the thresholds. Among these, the top 10 targets by degree values were AKT1 (degree = 100), TNF (98), IL6 (98), TP53 (95), IL1B (93), MMP9 (91), CASP3 (88), HIF1A (88), STAT3 (87), and ESR1 (87). In the network visualization, the node size and color intensity correspond to the number of interacting targets (Figure 3).

3.4. GO Function Analysis. GO annotation analysis of the 117 common targets was performed using the DAVID database, identifying 2,388 biological process (BP) entries, 65 cellular component (CC) entries, and 177 molecular function (MF) entries with $p < 0.05$. Terms were ranked by ascending p-value, and the top 10 entries for each category were visualized in bar charts (Figure 4a). The analysis showed that BP terms were predominantly enriched in response to lipopolysaccharide, bacterial molecules, and chemical stress (Figure 4b), CC terms were mainly localized to membrane raft regions (Figure 4c), and MF terms were significantly associated with gene expression regulation, protein modification and degradation, and cellular response to external signals (Figure 4d). Among them, the enrichment analysis values for response to lipopolysaccharide, membrane raft localization, and DNA-binding transcription factor binding were 4.58641×10^{-32}, 9.06903×10^{-14}, and 5.32247×10^{-15}, which were significantly lower than the 0.05 threshold. These results suggested that these functional categories may mediate the antifibrotic effects of FZHY in cirrhosis.

3.5. KEGG Pathway Enrichment Analysis. A total of 168 signaling pathways were identified in the KEGG signaling pathway analysis ($p < 0.05$). The top 10 pathways, ranked by ascending p-value, were visualized in a bar chart (Figure 5a). The pathway secondary classification summary results indicated that these common targets were associated with 21 secondary classifications, including signal transduction, cancer overview, and immune system (Figure 5b). The signal transduction category, which exhibited the highest number of enriched genes, was further analyzed through a bubble chart (Figure 5c). Key enriched pathways included the AGE-RAGE signaling pathway in diabetic complications (Figure 5d), the IL-17 signaling pathway, the TNF signaling pathway, and the PI3K-Akt signaling pathway. These findings suggested that genes within these pathways might mediate the antifibrotic effects of FZHY in cirrhosis.

3.6. Network Analysis of the Drug-Target-Disease-Pathway. The "drug-target-disease-pathway" network was constructed using Cytoscape 3.10.2 software, integrating common targets and enrichment results (Figure 6). The light-blue and pink triangles represent FZHY and cirrhosis, respectively. The common targets are shown as orange squares with a color intensity scaled by their degree centrality (darker colors indicating higher connectivity). The top 10 significantly enriched GO terms from biological process (BP), cellular component (CC), and molecular function (MF) analyses are visualized as pink, orange, and green diamonds, respectively. The top 20 signal transduction pathways identified through the Kyoto Encyclopedia of Genes and Genomes (KEGG) enrichment analysis with the smallest p-values are marked as purple hexagons. Node degrees of the common targets in the network were obtained by the Network Analyzer plugin (Cytoscape). Fourteen targets with the highest degree values were selected for the subsequent step of molecular docking (Tables 3 and S3). These targets were selected based on their central roles in bridging FZHY components, cirrhosis-related pathways, and functional annotations, suggesting their potential as key mediators of the formula's therapeutic effects.

3.7. Molecular Docking Results. In molecular docking, a lower binding energy indicates stronger binding and higher

https://doi.org/10.1021/acsomega.5c01225
ACS Omega 2025, 10, 19019−19032

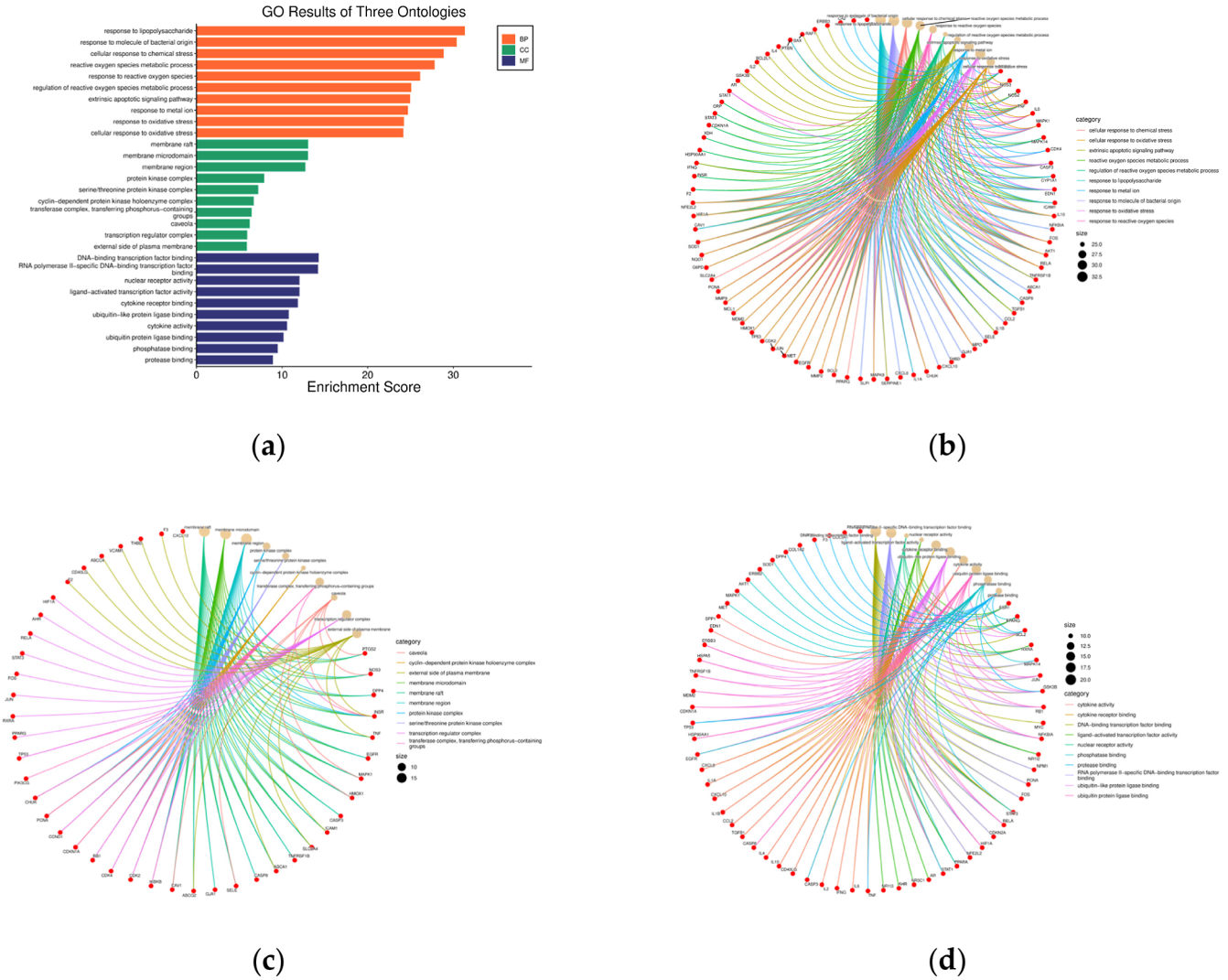

Figure 4. Gene Ontology (GO) enrichment analysis. (a) Integrated visualization of biological process (BP), molecular function (MF), and cellular component (CC) categories. (b) Top enriched biological processes. (c) Top enriched cellular components. (d) Top enriched molecular functions. The larger size of the node indicates greater enrichment of the GO terms in figure (b−d).

structural stability. A binding energy of ≤ −5.0 kcal/mol suggests potential interaction, while ≤ −7.0 kcal/mol implies robust binding.[14] Based on the PPI network, drug-target-disease-pathway network, and AGE-RAGE signaling pathway analysis, 14 key targets (Table 2) were docked with 12 active components (Table 1). Protein structures of the top 12 core targets (RELA, AKT1, TNF, MAPK8, CHUK, IKBKB, MAPK14, JUN, MAPK1, TP53, EGFR, IL6, STAT3, and BCL2) were retrieved from the Protein Data Bank (PDB) (Table 4). All key active components of FZHY exhibited binding energies ≤ −4.2 kcal/mol, with Isotanshinone II showing the strongest binding affinity for CHUK (−11.3 kcal/mol), IKBKB (−11.5 kcal/mol), and MAPK14 (−12.2 kcal/mol) (Figure 7 and Table S4). The six lowest-energy complexes were visualized using Discovery Studio 2021 software, revealing hydrogen bonds and other interactions formed between ligands and targets (Figure 8). These results supported the hypothesis that FZHY could exert anticirrhotic effects by modulating these targets.

3.8. Results of the Drug Sensitivity Assay Using the CCK-8 Method. Six concentrations of Isotanshinone II, Tanshinone IIA, Cryptotanshinone, and Quercetin were assessed for their effects on the proliferation of LX-2 cells, and the non-toxic dose was screened. As shown in Figure 9, Isotanshinone II exhibited cytotoxicity at concentrations >100 μM, while Tanshinone IIA and Quercetin required >400 μM, and Cryptotanshinone >800 μM. Therefore, based on the dosage reported in the literature and our cytotoxicity screening results,[15−17] we selected 12.5, 25, and 50 μM for Isotanshinone II, and 50, 100, and 200 μM for Tanshinone IIA, Cryptotanshinone, and Quercetin in subsequent experiments.

3.9. Effects of FZHY Components on COL1A1 and α-SMA Expressions in TGF-β-Induced LX-2 Cells. TGF-β could induce liver fibrosis, which would ultimately lead to cirrhosis. The mRNA expression levels of fibrotic markers (COL1A1 and α-SMA) in TGF-β-induced LX-2 cells were measured to assess the success of the fibrosis model and evaluate the antifibrotic effects of 4 key compounds. The results indicated that compared to the control group, TGF-β significantly upregulated the expression of COL1A1 and α-SMA (p < 0.01), confirming successful fibrosis modeling. Isotanshinone II dose-dependently reduced TGF-β-induced COL1A1 and α-SMA mRNA expression (p < 0.01, Figure 10A and B). Tanshinone IIA reduced COL1A1 expression in a dose-

https://doi.org/10.1021/acsomega.5c01225
ACS Omega 2025, 10, 19019−19032

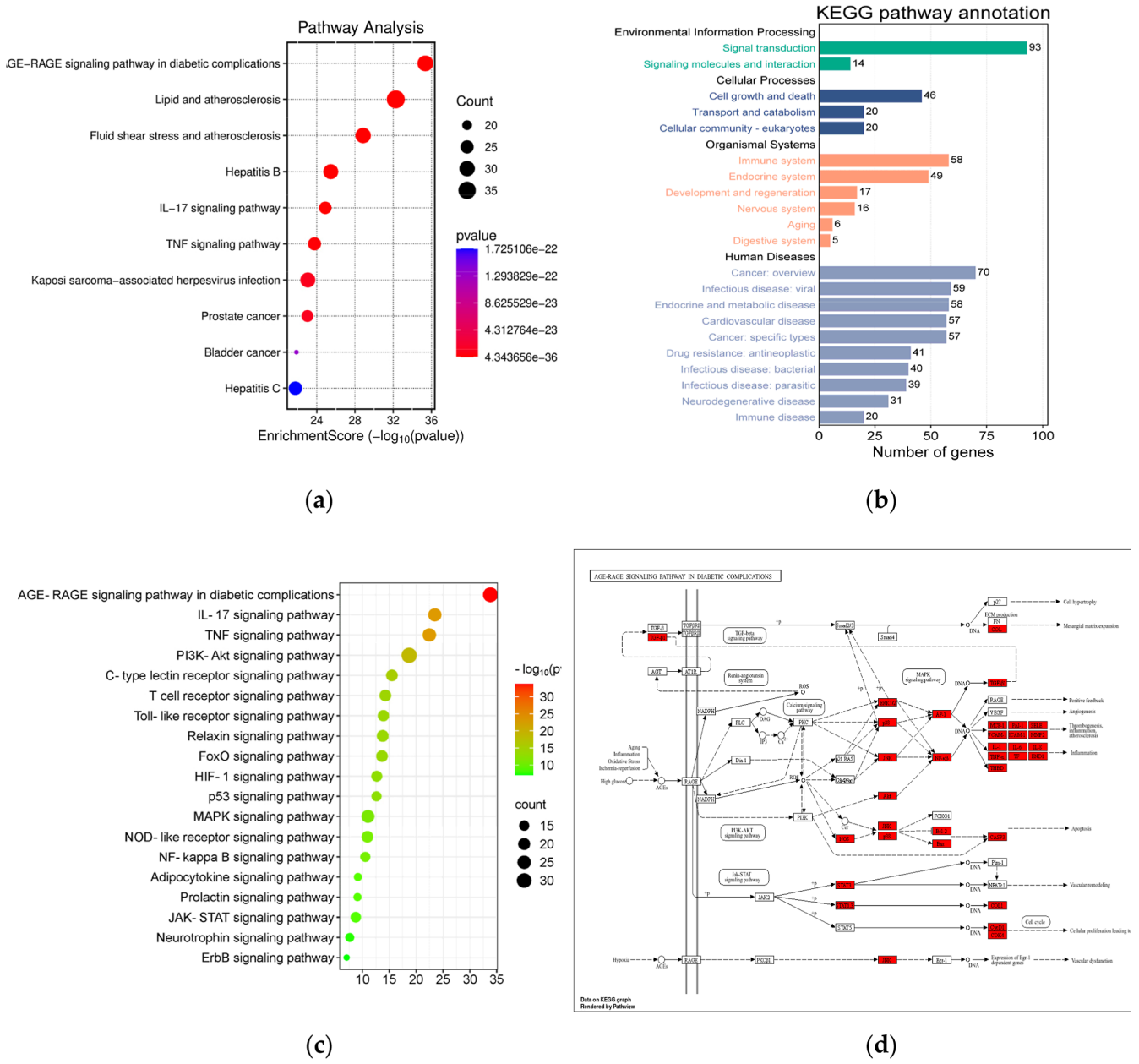

Figure 5. KEGG pathway enrichment analysis of key target genes. (a) Top 10 enriched pathways ranked by ascending *p*-value. Pathway names are displayed on the *x*-axis, with the *y*-axis indicating $-\log_{10}$ (*p*-value). Redder hues denote lower *p*-values (higher significance). (b) Secondary classification of pathways by functional categories. The *x*-axis shows the number of target genes in each pathway, and the *y*-axis lists the pathway categories. (c) Bubble plot of signal transduction pathways (node size: number of genes; color: *p*-value). (d) Molecular interaction network of the AGE-RAGE signaling pathway in diabetic complications.

dependent manner but inhibited α-SMA expression at only high doses. Cryptotanshinone had no significant effect on COL1A1 or α-SMA except at the highest dose ($p > 0.05$). Similarly, Quercetin showed no inhibitory effects on either marker. These results suggested that Isotanshinone II and Tanshinone IIA possessed potent antifibrotic activity in vitro, warranting further mechanistic investigation.

3.10. Effects on p38 MAPK, IKKβ, and NF-κB p65 Expressions in TGF-β-Induced LX-2 Cells. Based on PPI analysis and molecular docking results, p38 MAPK, IKKβ, and NF-κB p65 were identified as core proteins. As a key downstream pathway of MAPK signaling, the NF-κB signaling pathway was evaluated by measuring p38 MAPK, IKKβ, and NF-κB p65 protein expression in LX-2 cells coincubated with TGF-β1 and the compounds. The protein expression levels of p38 MAPK, IKKβ, and NF-κB p65 decreased in a dose-dependent manner in the Isotanshinone II groups (Figure 11). These findings indicated that Isotanshinone II effectively inhibited the activation of the MAPK/NF-κB pathway in LX-2 cells in vitro.

4. DISCUSSION

Cirrhosis, a severe consequence of chronic liver injury, leads to end-stage liver disease, with liver fibrosis being a key pathological precursor that disrupts the hepatic architecture. Recent studies highlight the significant potential of TCM in combating liver fibrosis, particularly FZHY, a recommended Chinese patent medicine.[5,18] Previous studies have reported that

https://doi.org/10.1021/acsomega.5c01225
ACS Omega 2025, 10, 19019−19032

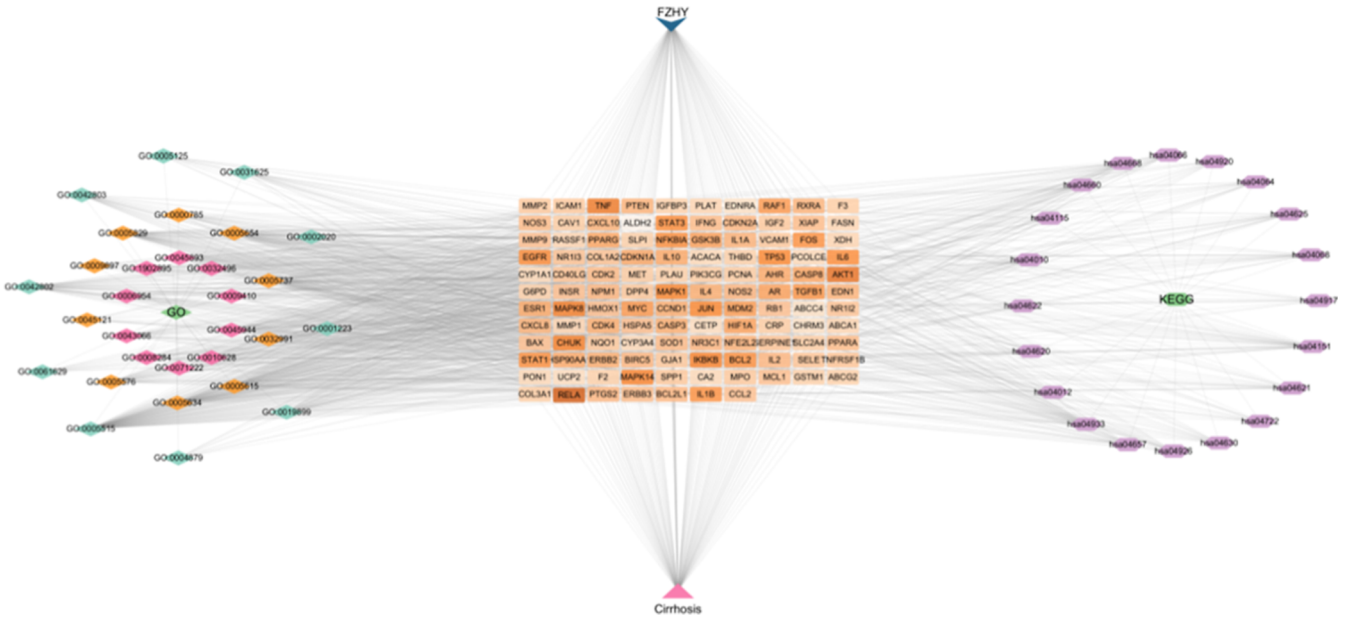

Figure 6. Overall network diagram of "drug-target-disease-pathway". The network contains 117 nodes and 2,841 edges. Orange squares represent genes, purple hexagons represent pathways, and pink/orange/green diamonds denote Gene Ontology (GO) enrichment analysis of biological process (BP), molecular function (MF), and cellular component (CC) analyses, respectively. The light-blue triangle represents Fuzheng Huayu, and the pink triangle represents cirrhosis.

Table 3. Top 14 Target Genes in Terms of Degree

gene name	betweenness centrality	closeness centrality	degree
RELA	0.023871072	0.537974684	38
AKT1	0.014657045	0.515151515	31
TNF	0.016348363	0.508982036	29
MAPK8	0.010840768	0.500000000	26
CHUK	0.010528193	0.500000000	26
IKBKB	0.010421102	0.497076023	25
MAPK14	0.009514205	0.497076023	25
JUN	0.009312843	0.494186047	24
MAPK1	0.008930768	0.494186047	24
TP53	0.009096299	0.494186047	24
EGFR	0.009191027	0.49132948	23
IL6	0.008224133	0.49132948	23
STAT3	0.009590767	0.49132948	23
BCL2	0.008665174	0.488505747	22

Table 4. Key Targets and Their High-Affinity Ligands in Molecular Docking

No.	receptor	identifier of the receptor	ligand	affinity (kcal/mol)
1	RELA	6YP8	tanshinone IIA	−8.6
2	AKT1	4GV1	tanshinone IIA	−9.6
3	TNF	2AZ5	isotanshinone II	−7.9
4	MAPK8	3PZE	isotanshinone II	−9.7
5	CHUK	5EBZ	isotanshinone II	−11.3
6	IKBKB	4KIK	isotanshinone II	−11.5
7	MAPK14	5OMH	isotanshinone II	−12.2
8	JUN	4KKH	isotanshinone II	−9.9
9	MAPK1	4QP9	isotanshinone II	−10.6
10	TP53	3ZME	quercetin	−8.4
11	EGFR	1ML7	cryptotanshinone	−9.9
12	IL6	5FUC	quercetin	−7.3
13	STAT3	6NJS	cryptotanshinone	−8.3
14	BCL2	2W3L	tanshinone IIA	−8

FZHY has been shown to reduce α-SMA levels in murine models of carbon tetrachloride (CCl_4) or dimethylnitrosamine (DMN)-induced liver fibrosis and improve histological outcomes in clinical trials, suggesting its efficacy in inhibiting fibrosis progression and reversing cirrhotic changes.[9,10,19−21] FZHY has also been reported to effectively reduce TNF-α and IL-6 levels in murine models of liver fibrosis.[22,23] In recent years, research has suggested that the improvement of liver injury and antiliver fibrosis by FZHY is related to its regulation of macrophage polarization.[12,24] Moreover, FZHY has demonstrated clinical benefits in hepatocellular carcinoma (HCC) patients by improving TNM stage and differentiation.[8] However, the specific anticirrhotic components and mechanisms of FZHY remain poorly understood. This study employs network pharmacology, molecular docking, and cellular experiments to elucidate the molecular mechanisms underlying FZHY's inhibitory effects on cirrhosis, providing a deeper scientific understanding of its therapeutic potential.

The network pharmacology analysis identified 10 active ingredients, including Quercetin, Tanshinone IIA, Cryptotanshinone, and Isotanshinone II, as well as 117 common targets between FZHY and cirrhosis, with 33 key targets exhibiting high connectivity and centrality in the PPI network. GO and KEGG enrichment analyses highlighted the involvement of the AGE-RAGE, MAPK, and NF-κB signaling pathways in cirrhosis (Figure 5d). Molecular docking demonstrated strong binding interactions between Quercetin, Tanshinone IIA, Cryptotanshinone, and Isotanshinone II to several key targets, particularly CHUK, IKBKB, and MAPK14, which are the core genes in MAPK and NF-κB signaling pathways. These findings suggest that the MAPK/NF-κB pathway may be central to FZHY's anticirrhotic effects.

The anti-fibrotic mechanisms of FZHY have been extensively studied, with a focus on HSC activation, a central driver of cirrhosis. HSCs' proliferation and transformation into myofibroblast-like cells, mediated by TGF-β, lead to excessive ECM

https://doi.org/10.1021/acsomega.5c01225
ACS Omega 2025, 10, 19019−19032

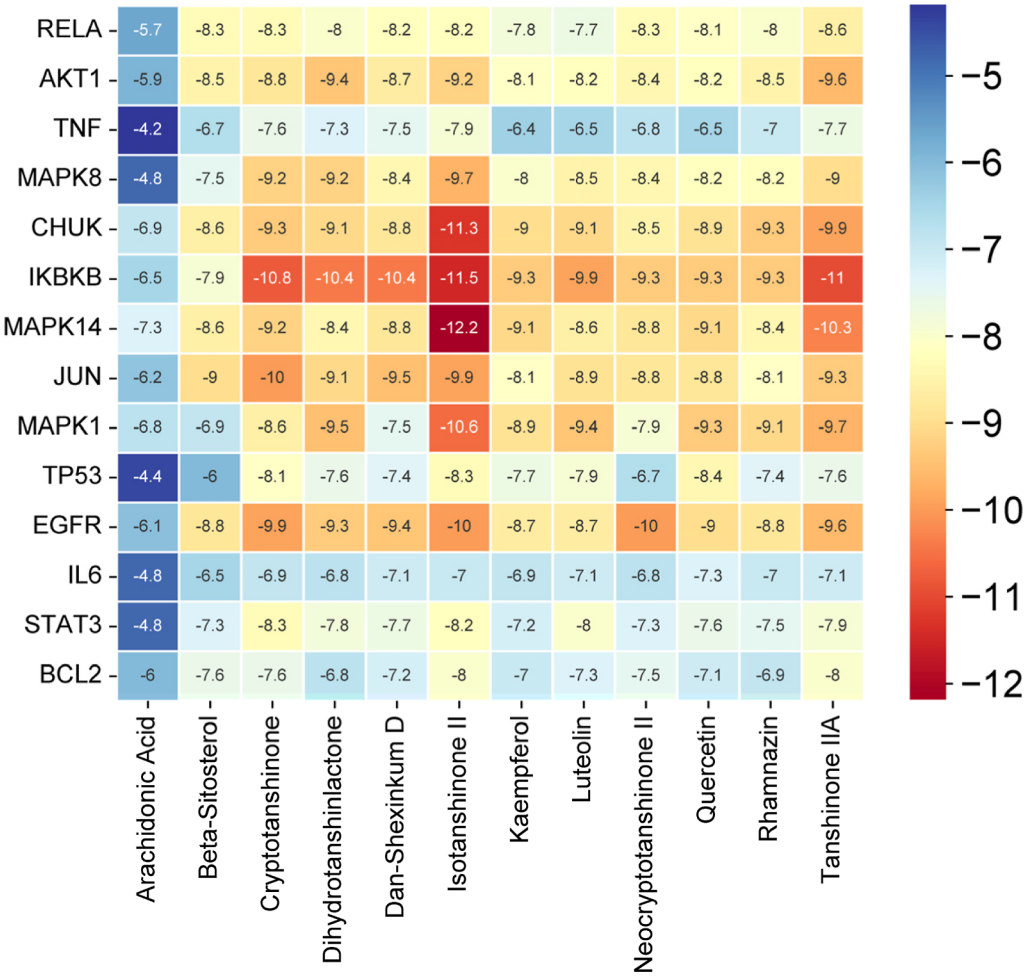

Figure 7. Heatmap of molecular docking scores for Fuzheng Huayu active compounds against key targets.

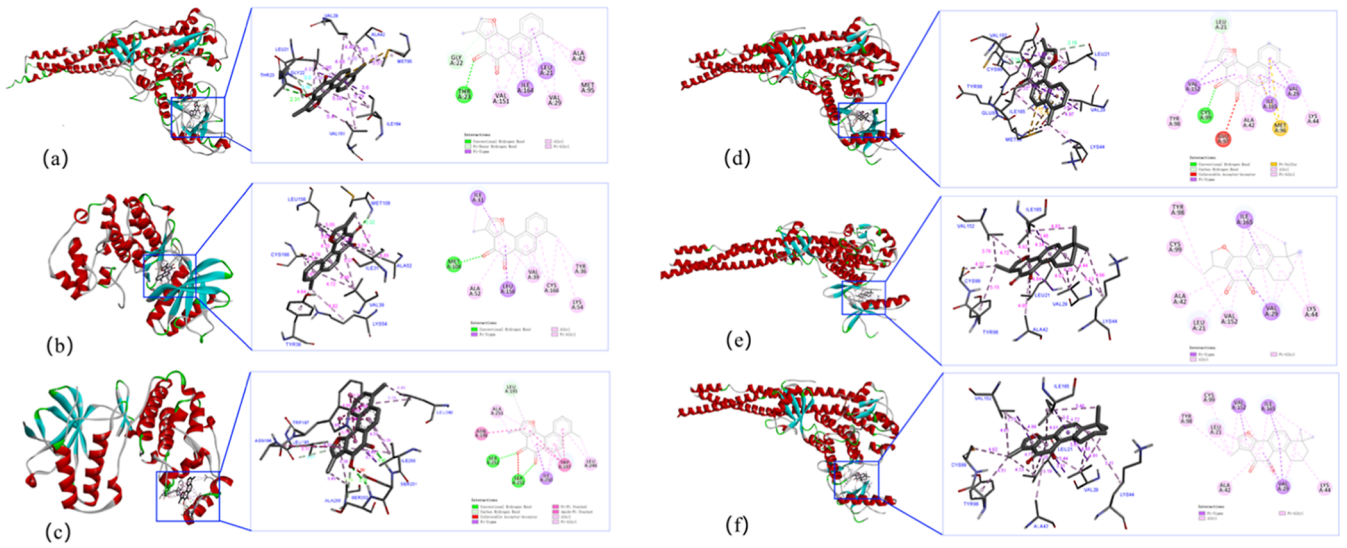

Figure 8. Binding modes between key targets and anti-cirrhotic compounds from Fuzheng Huayu. (a) CHUK-ISO. (b) MAPK1-ISO. (c) MAPK14-ISO. (d) IKBKB-ISO. (e) IKBKB-CTS. (f) IKBKB-TAN.

deposition, particularly collagen, which is pivotal in liver fibrosis progression. LX-2 cells, which retain key HSC characteristics, were used as an in vitro model to investigate these mechanisms.[25,26] FZHY has been shown to attenuate liver fibrosis by suppressing HSC activation, potentially through modulation of signaling pathways such as HIF-1, PI3K-Akt, and FoxO,[27] though further mechanistic elucidation is required. In this study, Isotanshinone II and Tanshinone IIA, active components of FZHY, significantly reduced TGF-β-induced COL1A1 and α-SMA mRNA levels, consistent with previous

https://doi.org/10.1021/acsomega.5c01225
ACS Omega 2025, 10, 19019−19032

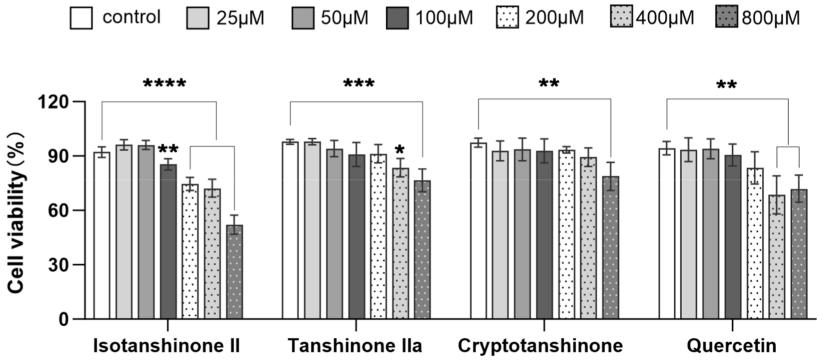

Figure 9. CCK-8 assay of LX-2 cells treated with Isotanshinone II, Tanshinone IIA, Cryptotanshinone, and Quercetin (drug concentration: 0−800 μmol/L). Data represent mean ± SD (n = 3). *p < 0.05, **p < 0.01, ***p < 0.001, ****p < 0.0001 vs the control group.

findings that FZHY-containing serum inhibits α-SMA expression and collagen synthesis in HSCs in a dose-dependent manner.[28] These results underscore the potent antifibrotic effects of these compounds in vitro, warranting further investigation to confirm their therapeutic potential.

Based on molecular docking results (Figure 7 and Table 3), p38 MAPK and IKKβ proteins, which are encoded by MAPK14 and IKBKB with lower binding energies, were selected for protein expression analysis. Additionally, the NF-κB p65 protein, corresponding to the RELA gene with the highest degree, as indicated in Table 2, was also selected for the protein expression measurement. Western blot analysis revealed that Isotanshinone II inhibited the phosphorylation of p38 MAPK, IKKβ, and NF-κB p65 in a concentration-dependent manner. In contrast, Tanshinone IIA did not show a significant effect on these key proteins. This result is consistent with the report by Wang et al.,[29] which showed FZHY significantly decreased the levels of IKK-β, NF-κB, and monocyte chemotactic protein 1 (MCP-1) in methionine and choline deficient L-amino acid diet-induced liver fibrosis mice. The differential effects of Isotanshinone II and Tanshinone IIa on these signaling pathways highlight the importance of structural specificity in the pharmacological activity of natural compounds, suggesting that Isotanshinone II may exert its antifibrotic effects by specifically modulating the MAPK/NF-κB signaling pathway through its unique molecular structure.

The mitogen-activated protein kinase (MAPK) cascade is a key signaling pathway that regulates the development of inflammation and liver fibrosis. Activation of this pathway in HSCs leads to the release of growth factors that stimulate the production of oxidative stress-related factors, promoting the proliferation of HSCs and ultimately accelerating liver fibrosis.[30−32] Among the MAPK subfamily, the p38 MAPK pathway is particularly significant, as its activation can lead to the upregulation of inflammatory responses, further exacerbating fibrotic processes.[33] The use of p38 MAPK inhibitors, such as FR-167653, has been shown to have a beneficial effect on liver cirrhosis by downregulating Runt-related transcription factor 2 (Runx2), suggesting that targeting the p38 MAPK pathway could be a potential therapeutic strategy for liver fibrosis and cirrhosis.[34] The NF-κB pathway also plays a pivotal role in regulating inflammation as its activation promotes the expression of pro-inflammatory cytokines and chemokines, which contribute to the inflammatory microenvironment in liver fibrosis.[35−39] Isotanshinone II in FZHY can exert its anti-fibrotic effects by modulating the MAPK/NF-κB signaling pathway. This inhibition disrupts the crosstalk between the MAPK and NF-κB pathways, which are known to synergistically drive inflammation and fibrogenesis. By suppression of these pathways, Isotanshinone II not only attenuates HSC activation but also mitigates the inflammatory microenvironment that perpetuates liver injury and fibrosis. Additionally, elucidating the precise molecular mechanisms by which Isotanshinone II interacts with p38 MAPK, IKKβ, and NF-κB p65 could provide insights into the design of more potent and selective inhibitors for clinical applications.

As mentioned in the literature review, the results of Fu et al., 2021,[40] and Chen et al., 2019,[41] showed that, among the ingredients of FZHY decoction, salvianolic acid B had the highest content, while amygdalin had the highest hepatic exposure, and schisandrin A exhibited maximum exposure in portal blood following oral administration. Tao et al. found that 11 components and two metabolites can be absorbed into blood in vivo, including salvianolic acid B, salvianolic acid G, cryptotanshinone I, cryptotanshinone II, miltirone I and tanshinol B, et al.[42] However, Isotanshinone II was not included. This compound, though identified in our study, was undetectable in animal bloodstream. The undetectability of Isotanshinone II in the bloodstream could be due to its rapid metabolism, low concentration, sample preparation issues, protein binding, analytical method limitations, or degradation. Each of these factors might contribute to the difficulty in detecting Isotanshinone II in blood samples, underscoring the need for further investigation into its pharmacokinetic properties.

Isotanshinone II, a bioactive component derived from Danshen (*Radix Salvia Miltiorrhiza*), exhibits diverse pharmacological effects, including anticancer activity, autophagy induction, cardiovascular and neuroprotection effects, as well as anti-inflammatory and antioxidant activities. Based on these pharmacological activities, we can enhance its bioavailability, efficacy, and safety through structural optimization. Additionally, advanced drug delivery systems, including nanoparticle-based carriers and liposomal formulations, could be developed to enhance their stability, prolong their circulation time, and improve their targeted delivery to specific tissues or cells. These innovations could not only address the current limitations in detecting and utilizing Isotanshinone II but also pave the way for its clinical application in treating conditions such as liver fibrosis and cancer.

5. CONCLUSIONS

Overall, this study demonstrated that FZHY exhibited significant anti-cirrhotic effects. Through network pharmacol-

https://doi.org/10.1021/acsomega.5c01225
ACS Omega 2025, 10, 19019−19032

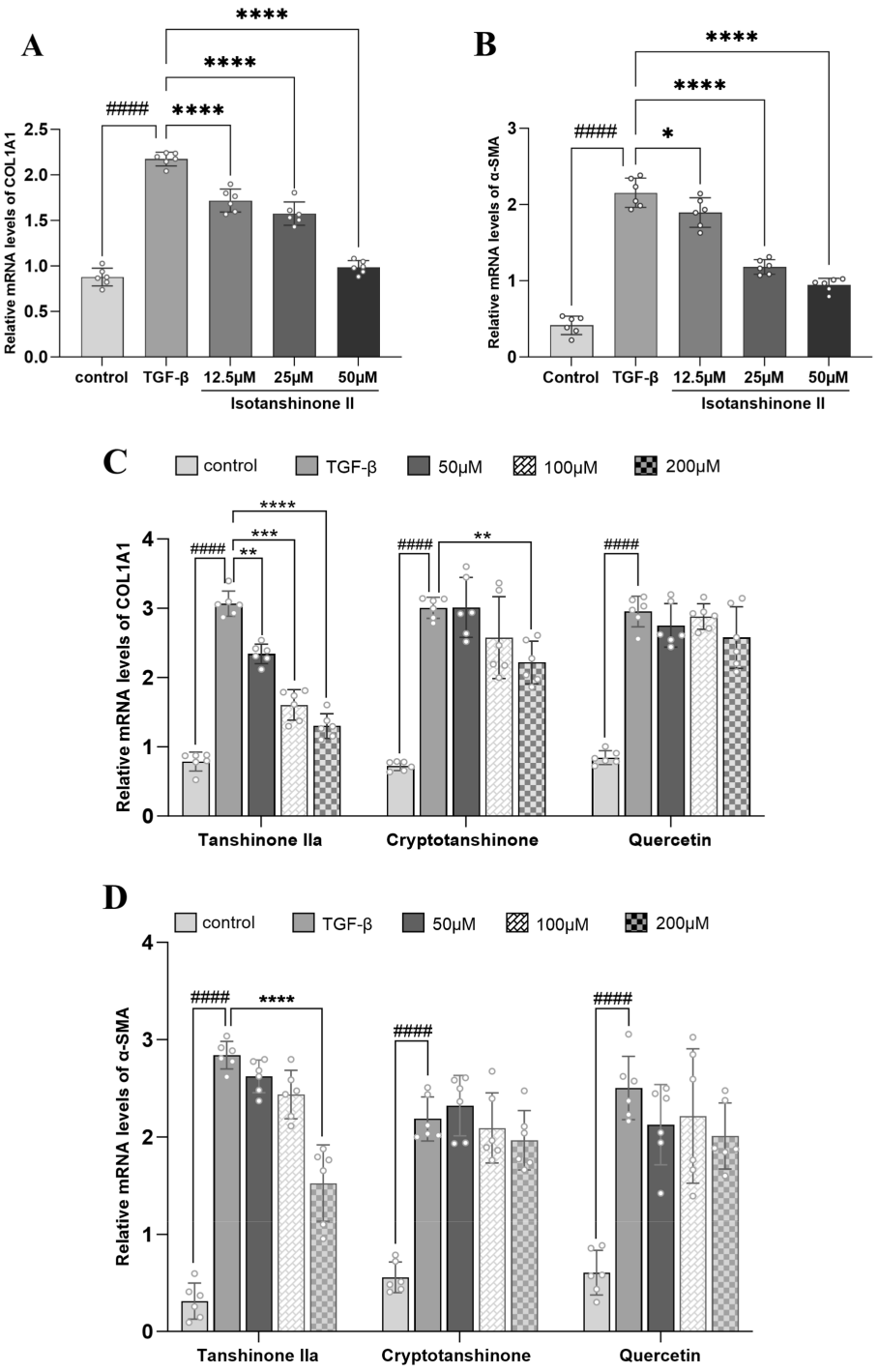

Figure 10. qRT-PCR analysis of COL1A1 and α-SMA mRNA expression in TGF-β-induced LX-2 cells treated with Fuzheng Huayu components. (A,C) Isotanshinone II and Tanshinone IIA dose-dependently reduce COL1A1 mRNA levels. (B,D) Dose-dependent inhibition of α-SMA mRNA by Isotanshinone II and Tanshinone IIA. Data represent mean ± SD ($n = 6$). Cryptotanshinone and Quercetin show no significant effects. *$p < 0.05$, **$p < 0.01$, ***$p < 0.001$, and ****$p < 0.0001$ vs TGF-β group; $^{\#\#\#\#}p < 0.0001$ vs control group.

ogy, molecular docking, and cell experiments, we identified several key active ingredients, including Isotanshinone II and Tanshinone IIA, and elucidated their mechanisms of action. FZHY primarily targeted the MAPK/NF-κB signaling pathway, which is crucial for the progression of liver fibrosis. Isotanshinone II, in particular, effectively inhibited HSC activation and reduced collagen production by regulating the phosphorylation of p38 MAPK, IKKβ, and NF-κB p65. These findings were consistent with previous studies highlighting the role of FZHY in modulating inflammation and macrophage polarization, further supporting its potential as a therapeutic agent for liver fibrosis. Despite the promising results, the study acknowledged its limitations. The absence of Isotanshinone II in blood samples suggested that further investigation was needed to explore its bioavailability and metabolism. Future research could focus on optimizing its structure, developing targeted drug delivery systems, and conducting in vivo experiments to validate the findings and assess its clinical applicability.

https://doi.org/10.1021/acsomega.5c01225
ACS Omega 2025, 10, 19019−19032

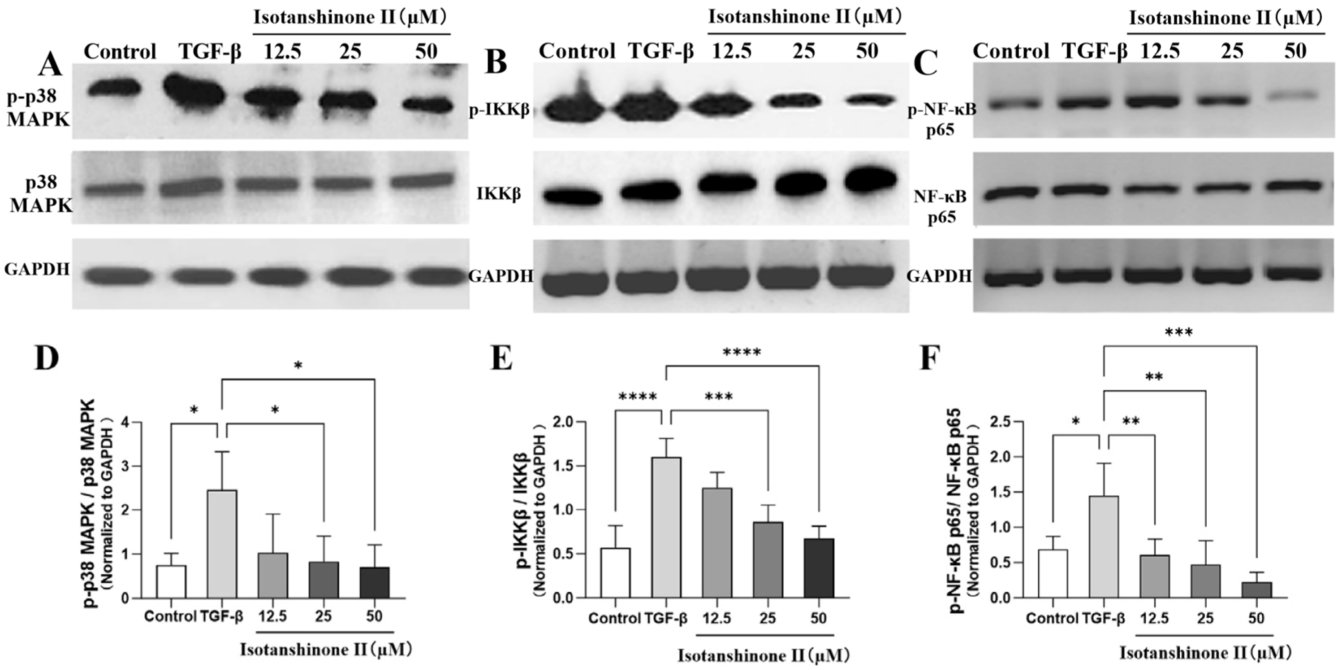

Figure 11. Western blot analysis results. (A−C) Representative images of Western blot analysis of p38 MAPK, IKKβ, and NF-κB p65. (D−F) Relative phosphorylation levels of p38 MAPK, IKKβ, and NF-κB p65. Isotanshinone II dose-dependently inhibits phosphorylation of p38 MAPK, IKKβ, and NF-κB p65 in TGF-β1-induced LX-2 cells. Data represent mean ± SD (n = 3). *p < 0.05, **p < 0.01, ***p < 0.001 vs the TGF-β group.

■ ASSOCIATED CONTENT

Supporting Information

The Supporting Information is available free of charge at https://pubs.acs.org/doi/10.1021/acsomega.5c01225.

Active components identified from each herb in FZHY; active ingredients in terms of degree; target genes in terms of degree; and molecular docking binding energies between the key components and key targets (PDF)

■ AUTHOR INFORMATION

Corresponding Author

Ruitao Yu − *Qinghai Provincial Key Laboratory of Tibetan Medicine Research, Northwest Institute of Plateau Biology, Chinese Academy of Sciences, Xining 810008, China;* orcid.org/0000-0001-7500-4565; Phone: +86-0971-6143530; Email: yuruitao@nwipb.cas.cn

Authors

Ruixue Yu − *Medicine College of Pingdingshan University, Pingdingshan 467000, China;* orcid.org/0000-0002-3863-2455

Run Shi − *Medicine College of Pingdingshan University, Pingdingshan 467000, China*

Jinghua Chen − *Northwest Institute of Plateau Biology, Chinese Academy of Sciences, Xining 810008, China*

Xinhua Zheng − *Medicine College of Pingdingshan University, Pingdingshan 467000, China*

Complete contact information is available at: https://pubs.acs.org/10.1021/acsomega.5c01225

Author Contributions

Experiment design: R.T.Y. Experiment operation: R.X.Y., R.S., J.H.C. Data statistics: R.X.Y., X.H.Z. Writing: R.X.Y., R.S., J.H.C. Review and editing: R.T.Y. Funding acquisition, R.T.Y., X.H.Z., R.S. All authors have read and approved the final version.

Notes

The authors declare no competing financial interest.

■ ACKNOWLEDGMENTS

This research was funded by the Qinghai Province Central Government Guides Local Science and Technology Development Fund (No. 2025ZY014 to R.Y.), Interinstitute Joint Fund of Lanzhou Branch of the Chinese Academy of Sciences (No. E4291212 to R.Y.), and Key Scientific Research Projects of Higher Education Institutions in Henan Province (No. 25A180026 to R.S.), Pingdingshan University Young Backbone Faculty Support Program (No. 53 [2022] to R.Y.).

■ REFERENCES

(1) Angeli, P.; Bernardi, M.; Villanueva, C.; Francoz, C.; Mookerjee, R. P.; Trebicka, J.; Krag, A.; Laleman, W.; Gines, P. EASL Clinical Practice Guidelines for the management of patients with decompensated cirrhosis. *J. Hepatol.* **2018**, *69* (2), 406−460.

(2) Yoshiji, H.; Nagoshi, S.; Akahane, T.; Asaoka, Y.; Ueno, Y.; Ogawa, K.; Kawaguchi, T.; Kurosaki, M.; Sakaida, I.; Shimizu, M.; et al. Evidence-based clinical practice guidelines for Liver Cirrhosis 2020. *J. Gastroenterol.* **2021**, *56* (7), 593−619.

(3) Huang, D. Q.; Terrault, N. A.; Tacke, F.; Gluud, L. L.; Arrese, M.; Bugianesi, E.; Loomba, R. Global epidemiology of cirrhosis-aetiology, trends and predictions. *Nat. Rev. Gastroenterol. Hepatol.* **2023**, *20* (6), 388−398.

(4) Ginès, P.; Krag, A.; Abraldes, J. G.; Solà, E.; Fabrellas, N.; Kamath, P. S. Liver cirrhosis. *Lancet* **2021**, *398* (10308), 1359−1376.

(5) Zhou, X. X.; Fu, Y. D.; Chen, J. M.; Liu, P. Progress in clinical and basic research of fuzheng Huayu formula for the treatment of liver fibrosis. *J. Ethnopharmacol.* **2024**, *327*, 118018.

(6) Li, H. Advances in anti hepatic fibrotic therapy with Traditional Chinese Medicine herbal formula. *J. Ethnopharmacol.* **2020**, *251*, 112442.

(7) Zhu, H.; Du, Z.; Lu, R.; Zhou, Q.; Shen, Y.; Jiang, Y. Investigating the Mechanism of Chufan Yishen Formula in Treating Depression through Network Pharmacology and Experimental Verification. *ACS Omega* **2024**, *9* (11), 12698−12710.

(8) Liu, H. L.; Lv, J.; Zhao, Z. M.; Xiong, A. M.; Tan, Y.; Glenn, J. S.; Tao, Y. Y.; Weng, H. L.; Liu, C. H. Fuzhenghuayu Decoction ameliorates hepatic fibrosis by attenuating experimental sinusoidal capillarization and liver angiogenesis. *Sci. Rep.* **2019**, *9* (1), 18719.
(9) Zhao, Z. M.; Zhu, C. W.; Huang, J. Q.; Li, X. D.; Zhang, Y. X.; Liang, J.; Zhang, W.; Zhang, Y.; Jiang, X. G.; Zong, Y. L.; et al. Efficacy and safety of Fuzheng Huayu tablet on persistent advanced liver fibrosis following 2 years entecavir treatment: a single arm clinical objective performance criteria trial. *J. Ethnopharmacol.* **2022**, *298*, 115599.
(10) Zhang, W. Q.; Sun, J. X.; Lan, S. T.; Sun, X. M.; Guo, Y. J.; Wen, B. C.; Chen, J.; Liu, G. Regulation of Fuzheng Huayu capsule on inhibiting the fibrosis-associated hepatocellular carcinogenesis. *J. Asian Nat. Prod. Res.* **2024**, *26* (10), 1219−1238.
(11) Ping, D. B.; Qi, J. S.; Li, M.; Sun, X.; Peng, Y.; Liu, C. H. Fuzheng Huayu recipe alleviates liver fibrosis via inhibiting NLRP3 inflammasome activation in macrophages. *J. Ethnopharmacol.* **2024**, *318* (Pt B), 117001.
(12) Zhang, W.; Guo, H.; Li, L.; Zhang, M.; Xu, E.; Dai, L. Network Pharmacology-Based Strategy Integrated with Molecular Docking and In Vitro Experimental Validation to Explore the Underlying Mechanism of Fangji Huangqi Decoction in Treating Rheumatoid Arthritis. *ACS Omega* **2024**, *9* (29), 31878−31889.
(13) Chang, C.; Zhen Yang, Z.; Sen Song, Y.; Gao, Na.; Zhe Zhang, H.; Lin Zhang, X.; Li Fan, T. Unveiling the mechanism of Buddleja officinalis against esophageal squamous cell carcinoma through network pharmacology and molecular docking approaches. *Tumor Discovery* **2024**, *3* (1), 2312.
(14) Wang, X. Y.; Yan, C. H.; Wang, T.; Li, Y. J.; Zheng, Z. Y. Mechanisms of Luteolin Against Gastro-Esophageal Reflux Disease Based on Network Pharmacology, Molecular Docking, and Molecular Dynamics Simulation. *Cell Biochem. Biophys.* **2025**, *83* (1), 403−414.
(15) Feng, M. C.; Luo, F.; Huang, L. J.; Li, K.; Chen, Z. M.; Li, H.; Yao, C.; Qin, B. J.; Chen, G. Z. Rheum palmatum L. and Salvia miltiorrhiza Bge. Alleviates Acute Pancreatitis by Regulating Th17 Cell Differentiation: An Integrated Network Pharmacology Analysis, Molecular Dynamics Simulation and Experimental Validation. *Chin. J. Integr. Med.* **2024**, *30* (5), 408−420.
(16) Roth, A.; Zhao, P.; Soukup, S. T.; Guigas, C.; Stärke, J.; Kulling, S. E.; Diel, P. Chemical Stability and Bioactivity of tanshinone I, tanshinone IIA, cryptotanshinone and dihydrotanshinone in in vitro test systems. *Toxicol. Lett.* **2023**, *375*, 21−28.
(17) Shakerian, E.; Afarin, R.; Akbari, R.; Mohammadtaghvaei, N. Effect of Quercetin on the fructose-activated human hepatic stellate cells, LX-2, an in-vitro study. *Mol. Biol. Rep.* **2022**, *49* (4), 2839−2845.
(18) Dai, Y. K.; Fan, H. N.; Zhao, Z. M.; Shen, L.; Liu, C. H. Syndrome of liver depression and spleen deficiency is a primary TCM syndrome of response to entecavir + FuZheng HuaYu in patients with HBV-related liver fibrosis. *Heliyon* **2023**, *9* (11), No. e22216.
(19) Cheng, Q.; Li, N.; Chen, M.; Zheng, J.; Qian, Z.; Wang, X.; Huang, C.; Li, Q.; Lin, Q.; Shi, G. Fuzheng Huayu inhibits carbon tetrachloride-induced liver fibrosis in mice through activating hepatic NK cells. *J. Ethnopharmacol.* **2013**, *145* (1), 175−181.
(20) Cheng, D. Y.; Zhao, Z. M.; Wan, G.; Zheng, H. W.; Huang, J. Q.; Liu, C. H.; Xing, H. C. Impact of Fuzheng Huayu tablet on antiviral effect of entecavir in patients with hepatitis B cirrhosis. *Hepatobiliary Pancreat. Dis. Int.* **2022**, *21* (5), 479−484.
(21) Pan, Q.; Wang, Y. Q.; Li, G. M.; Duan, X. Y.; Fan, J. G. Fuzheng huayu recipe ameliorates liver fibrosis by restoring balance between epithelial-to-Mesenchymal transition and mesenchymal-to-Epithelial transition in hepatic stellate cells. *BioMed Res. Int.* **2015**, *2015*, 935903.
(22) Jia, Y. H.; Wang, R. Q.; Mi, H. M.; Kong, L. B.; Ren, W. G.; Li, W. C.; Zhao, S. X.; Zhang, Y. G.; Wu, W. J.; Nan, Y. M.; Yu, J. Fuzheng Huayu recipe prevents nutritional fibrosing steatohepatitis in mice. *Lipids Health Dis.* **2012**, *11*, 45.
(23) Tao, Y. Y.; Yan, X. C.; Zhou, T.; Shen, L.; Liu, Z. L.; Liu, C. H. Fuzheng Huayu recipe alleviates hepatic fibrosis via inhibiting TNF-α induced hepatocyte apoptosis. *BMC Compl. Alternative Med.* **2014**, *14*, 449.
(24) Yang, T.; Liu, S.; Wang, C. H.; Tao, Y. Y.; Zhou, H.; Liu, C. H. Comparative pharmacokinetic and tissue distribution profiles of four major bioactive components in normal and hepatic fibrosis rats after oral administration of Fuzheng Huayu recipe. *J. Pharm. Biomed. Anal.* **2015**, *114*, 152−158.
(25) Xu, L.; Hui, A. Y.; Albanis, E.; Arthur, M. J.; O'Byrne, S. M.; Blaner, W. S.; Mukherjee, P.; Friedman, S. L.; Eng, F. J. Human hepatic stellate cell lines, LX-1 and LX-2: new tools for analysis of hepatic fibrosis. *Gut* **2005**, *54* (1), 142−151.
(26) Jiang, N.; Zhang, J.; Ping, J.; Xu, L. Salvianolic acid B inhibits autophagy and activation of hepatic stellate cells induced by TGF-β1 by downregulating the MAPK pathway. *Front. Pharmacol* **2022**, *13*, 938856.
(27) Jiang, C. Y.; Iwaisako, K.; Cong, M.; Diggle, K.; Hassanein, T.; Brenner, D. A.; Kisseleva, T. Traditional Chinese medicine fuzheng huayu prevents development of liver fibrosis in mice. *Arch. Clin. Biomed. Res.* **2020**, *04* (05), 561−580.
(28) Liu, C.; Hu, Y.; Xu, L.; Liu, C.; Liu, P. Effect of Fuzheng Huayu formula and its actions against liver fibrosis. *Chin. Med.* **2009**, *4*, 12.
(29) Wang, R.-Q.; Mi, H. M.; Li, H.; Zhao, S. X.; Jia, Y. H.; Nan, Y. M. Modulation of IKKβ/ NF-κB and TGF-β1/Smad via Fuzheng Huayu recipe involves in prevention of nutritional steatohepatitis and fibrosis in mice. *Iran. J. Basic Med. Sci.* **2015**, *18* (4), 404−411.
(30) Wang, Y.; Song, J. Y.; Bian, H. Y.; Bo, J. Q.; Lv, S. Y.; Pan, W. T.; Lv, X. R. Apelin promotes hepatic fibrosis through ERK signaling in LX-2 cells. *Mol. Cell. Biochem.* **2019**, *460* (1−2), 205−215.
(31) Wang, R.; Zhang, H.; Wang, Y. Y.; Song, F. X.; Yuan, Y. F. Inhibitory effects of quercetin on the progression of liver fibrosis through the regulation of NF-κB/ IκBα, p38 MAPK, and Bcl-2/Bax signaling. *Int. Immunopharmacol.* **2017**, *47*, 126−133.
(32) Su, G. Y.; Li, Z. Y.; Wang, R.; Lu, Y. Z.; Nan, J. X.; Wu, Y. L.; Zhao, Y. Q. Signaling pathways involved in p38- ERK and inflammatory factors mediated the anti-fibrosis effect of AD-2 on thioacetamide-induced liver injury in mice. *Food Funct.* **2019**, *10* (7), 3992−4000.
(33) Huo, S.; Li, B.; Du, J.; Zhang, X.; Zhang, J.; Wang, Q.; Song, M.; Li, Y. Dibutyl phthalate induces liver fibrosis via p38MAPK/NF-κB/NLRP3-mediated pyroptosis. *Sci. Total Environ.* **2023**, *897*, 165500.
(34) Hattori, S.; Dhar, D.; Hara, N.; Tonomoto, Y.; Onoda, T.; Ono, T.; Yamanoi, A.; Tachibana, M.; Tsuchiya, M.; Nagasue, N. FR-167653, a selective p38 MAPK inhibitor, exerts salutary effect on liver cirrhosis through downregulation of Runx2. *Lab. Invest.* **2007**, *87* (6), 591−601.
(35) Lei, J.-q.; Xie, Q. L.; Li, Q. P.; Qin, S. Y.; Wu, J. H.; Jiang, H. X.; Yu, B.; Luo, W. Resveratrol Alleviates Liver Fibrosis by Targeting Cross-Talk Between TLR2/MyD88/ERK and NF-κB/NLRP3 Inflammasome Pathways in Macrophages. *J. Biochem. Mol. Toxicol.* **2025**, *39* (3), No. e70208.
(36) Zhang, K.; Zhang, M. X.; Meng, X. X.; Zhu, J.; Wang, J. J.; He, Y. F.; Li, Y. H.; Zhao, S. C.; Shi, Z. M.; Zheng, L. N.; Han, T.; Hong, W. Targeting GPR65 alleviates hepatic inflammation and fibrosis by suppressing the JNK and NF-κB pathways. *Mil. Med. Res.* **2023**, *10* (1), 56.
(37) Taru, V.; Szabo, G.; Mehal, W.; Reiberger, T. Inflammasomes in chronic liver disease: Hepatic injury, fibrosis progression and systemic inflammation. *J. Hepatol.* **2024**, *81* (5), 895−910.
(38) Li, H.; Hu, P.; Zou, Y.; Yuan, L.; Xu, Y.; Zhang, X.; Luo, X.; Zhang, Z. Tanshinone IIA and hepatocellular carcinoma: A potential therapeutic drug. *Front. Oncol.* **2023**, *13*, 1071415.
(39) Tacke, F.; Trautwein, C. Mechanisms of liver fibrosis resolution. *J. Hepatol.* **2015**, *63* (4), 1038−1039.
(40) Fu, Y.; Xiao, Z.; Tian, X.; Liu, W.; Xu, Z.; Yang, T.; Hu, Y.; Zhou, X.; Fang, J.; Gao, S.; et al. The novel Chinese medicine JY5 formula alleviates hepatic fibrosis by inhibiting the Notch signaling pathway. *Front. Pharmacol* **2021**, *12*, 671152.
(41) Chen, J.; Hu, Y.; Chen, L.; Liu, W.; Mu, Y.; Liu, P. The effect and mechanisms of Fuzheng Huayu formula against chronic liver Diseases. *Biomed. Pharmacother.* **2019**, *114*, 108846.
(42) Yang, T.; Shen, D. P.; Wang, Q. L.; Tao, Y. Y.; Liu, C. H. Investigation of the absorbed and metabolized components of Danshen

https://doi.org/10.1021/acsomega.5c01225
ACS Omega 2025, 10, 19019−19032

from Fuzheng Huayu recipe and study on the anti-hepatic fibrosis effects of these components. *J. Ethnopharmacol.* **2013**, *148*, 691−700.

NOTE ADDED AFTER ASAP PUBLICATION

Due to a production error, the version of this paper that was published ASAP April 29, 2025, contained errors in the author affiliations. The corrected version was posted April 30, 2025.

https://doi.org/10.1021/acsomega.5c01225
ACS Omega 2025, 10, 19019−19032